Article

Transition-Metal Nanocluster Size vs Formation Time and the Catalytically Effective Nucleus Number: A Mechanism-Based Treatment

Murielle A. Watzky, Eric E. Finney, and Richard G. Finke

J. Am. Chem. Soc., **2008**, 130 (36), 11959-11969 • DOI: 10.1021/ja8017412 • Publication Date (Web): 16 August 2008

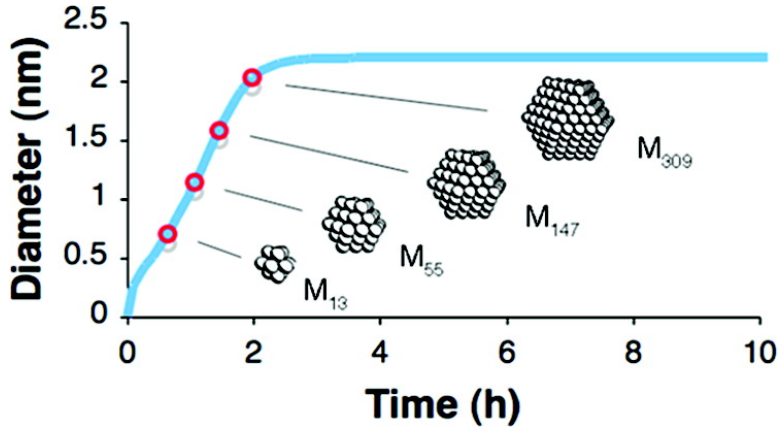

More About This Article

Additional resources and features associated with this article are available within the HTML version:

- Supporting Information
- Access to high resolution figures
- Links to articles and content related to this article
- Copyright permission to reproduce figures and/or text from this article

View the Full Text HTML

J|A|C|S
ARTICLES

Published on Web 08/16/2008

Transition-Metal Nanocluster Size vs Formation Time and the Catalytically Effective Nucleus Number: A Mechanism-Based Treatment

Murielle A. Watzky, Eric E. Finney, and Richard G. Finke*

Department of Chemistry, Colorado State University, Fort Collins, Colorado 80523

Received March 11, 2008; E-mail: finke@lamar.colostate.edu

Abstract: A mechanism-based equation for the size of a forming transition-metal nanocluster vs time has been derived based on the Finke−Watzky two-step mechanism for transition-metal nanocluster nucleation ($A \rightarrow B$, rate constant k_1) and autocatalytic growth ($A + B \rightarrow 2B$, rate constant k_2), where A is the nanocluster precursor and B is the growing nanocluster. The resultant equation expresses nanocluster diameter as a function of time, D_t, in terms of k_1, k_2, the initial concentration of the nanocluster precursor complex, $[A]_0$, and the number of catalytically effective nuclei derived from either (i) the final nanocluster size, D_f, or (ii) the number of atoms in the *average* catalytically effective nucleus, N^*, and the induction period time, t_{ind} (N^* being by definition the number of atoms present in the average size nucleus at the end of the induction period and when observable catalysis begins). By fitting experimentally determined nanocluster size vs time data using this equation, evidence for the validity of the equation is obtained for Ir^0 nanoclusters formed from the well-studied system of H_2 reduction of the precursor $[(1,5\text{-COD})Ir\cdot P_2W_{15}Nb_3O_{62}]^{8-}$. The D_t equation is then used to determine N^* for nine prior Ir^0 nanocluster preparations from five different $[(1,5\text{-COD})Ir^+]_n[anion^{n-}]$ precursors. Also given is a relationship allowing one to interconvert between nanocluster size data and nanocluster precursor concentration data, again when the two-step nucleation and growth mechanism has been shown to apply. Some of the key experimental factors that are known to affect the kinetics of nanocluster formation, and therefore nanocluster size, are also summarized. A look ahead to needed future work is also provided.

Introduction

One of the major goals of nanocluster science—the control over nanocluster size—is important since, at the nanoscale, cluster properties are highly sensitive to size. The properties that are most often studied as useful applications of nanoclusters include electronics,[1] magnetics,[2] optics,[3] and catalysis.[4] Having control over these properties by controlling nanocluster size[5] has, therefore, become a "Holy Grail" of the field along with control over nanocluster shape as well as composition.[6]

Nanoclusters of predetermined size have been prepared by a variety of mostly physical template (e.g., micelle or other template) methods[7] as well as seeding methods.[8,9] Prior studies attempting to relate nanocluster formation kinetics to size do exist.[10,11] However, in a 2004 study only nanocluster growth is treated kinetically—that is, the crucial nucleation step is ignored—and a likely incorrect linear diffusional growth is assumed rather than employing the now well-established step of autocatalytic surface-growth.[12] A second interesting 2007 study by Kumar, Gandhi, and Kumar[11] looks at Turkevich's classic $AuCl_3$/citrate^{3-} nanocluster preparation method and the $Au^0{}_n$ nanocluster size vs citrate^{3-}/$AuCl_3$ data obtained over 50 years by four different groups (Figure 1 therein[11]). Unfortunately, this work, too, proceeds from assumed stoichiometries and mechanistic steps, although it does yield a reasonable fit to

(1) Van Buren, T.; Dinh, L. N.; Chase, L. L.; Siekhaus, W. J.; Terminello, L. J. *Phys. Rev. Lett.* **1998**, *80*, 3803.
(2) Nakayama, T.; Yamamoto, T. A.; Choa, Y.-H.; Niihara, K. *J. Mater. Sci.* **2000**, *35*, 3857.
(3) Magruder, R. H., III; Haglund, R. F., Jr.; Yang, L.; Wittig, J. E.; Zuhr, R. A. *J. Appl. Phys.* **1994**, *76*, 708.
(4) Che, M.; Bennett, C. O. *Adv. Catal.* **1989**, *36*, 55.
(5) Corain, B.; Schmid, G.; Toshima, N., Eds. *Metal Nanoclusters in Catalysis and Materials Sciences: The Issue of Size Control*; Elsevier: Amsterdam, 2008.
(6) Starkey-Ott, L.; Finke, R. G. *Coord. Chem. Rev.,* **2007**, *251*, 10751100. One key conclusion of this review is the need for, and current lack of, composition information on transition-metal nanoclusters.

(7) (a) Prior nanocluster size control typically involves some kind of template to physically limit the growth of the clusters to a particular size. These templates include inverse micelles, resins, gels, and cages.[7c−g] For example, Pileni has prepared nanoclusters of Au[7b] and Cu[7c] in reverse micelles, using H_2O concentration to control the size of the clusters (larger clusters were obtained at higher H_2O concentration). Microgels[7d] and resins[7e,f] have also been used as templates with success, resulting in size-controlled supported nanoclusters. Using a sol−gel method to prepare TiO_2 nanoclusters, it was found that lowering the pH of the reaction system led to smaller clusters.[7g] The use of dendrimers is also common,[7h] larger nanoclusters being formed in larger, later-generation dendrimers. Pd clusters formed in an apoferritin cage to control their size were found to be active in the hydrogenation of alkenes[7i]. (b) Petit, C.; Lixon, P.; Pelini, M. P. *J. Phys. Chem.* **1993**, *97*, 12974. (c) Lisiecki, I.; Pileni, M. P. *J. Am. Chem. Soc.* **1993**, *115*, 3887. (d) Biffis, A.; Orlandi, N.; Corain, B. *Adv. Mater.* **2003**, *15*, 1551. (e) Corain, B.; Jerabek, K.; Centomo, P.; Canton, P. *Angew. Chem., Int. Ed.* **2004**, *43*, 959. (f) Centomo, P.; Zecca, M.; Corain, B. *J. Cluster Sci.* **2007**, *18*, 947. (g) Sugimoto, T.; Xingping, Z. *J. Colloid Interface Sci.* **2002**, *252*, 347. (h) D'Aléol, A.; Williams, R. M.; Osswald, F.; Edamana, P.; Hahn, U.; van Heyst, J.; Tichelaar, F. D.; Vögtle, F.; De Cola, L. *Adv. Funct. Mater.* **2004**, *14*, 1167. (i) Ueno, T.; Suzuki, M.; Goto, T.; Matsumoto, T.; Nagayama, K.; Watanabe, Y. *Angew. Chem., Int. Ed.* **2004**, *43*, 2527.

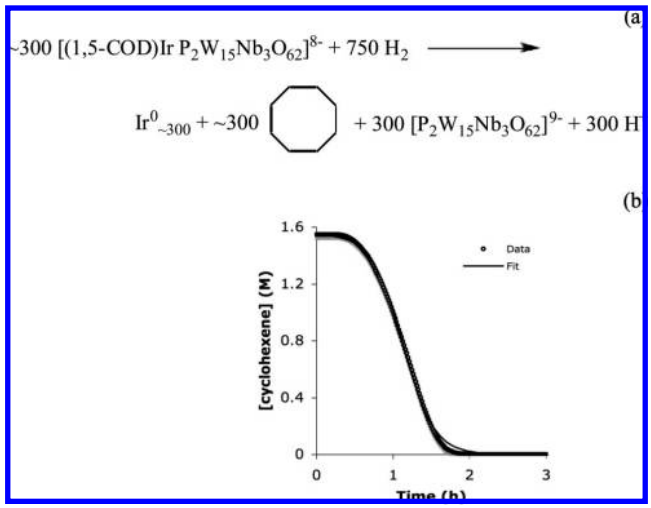

Figure 1. (a) Established balanced stoichiometry for H_2 reduction of the polyoxoanion-supported Ir complex $[Bu_4N]_5Na_3[(1,5\text{-COD})Ir\cdot P_2W_{15}Nb_3O_{62}]$ in acetone and with cyclohexene present to form, on average, $Ir^0_{\sim 300}$ nanoclusters for the specific conditions employed (see the Experimental Section). The nanoclusters are then good cyclohexene hydrogenation catalysts so that their formation can be followed indirectly, but in real time, by their hydrogenation activity and the pseudoelementary step method summarized by eqs 1a−d. (b) Observed kinetic curve for cyclohexene loss, and by eq 1d, the desired conversion of A into B. The fit shown is to the two-step, mechanism in Scheme 1 of A → B and A + B → 2B, with resultant $k_1 = 0.022(1)\ h^{-1}$ and $k_2 = 4.28(6) \times 10^3\ M^{-1}\ h^{-1}$.

the nanocluster size vs citrate^{3-}/$AuCl_3$ data. Perhaps most significantly, those authors use a so-called number- or population-balance approach to estimate the number density (concentration) of particles.[11,13] A valuable study by W. Yang, X. Peng, and co-workers examines the effects of the Na_3[citrate^{3-}]/$HAuCl_4$ ratio on the size of Au_n nanoclusters made in water at 100 °C in a version of Turkevich's classic synthesis. They found that it is actually the pH and pH-dependent speciation, $[AuCl_{4-x}(OH)_x]^-$ ($x = 0$ at pH 3.3 to $x = 3$ at pH 8.1), that are the underlying key variables in that complicated system.[14]

However, to date, no prior study uses a kinetically verified mechanism fortified by a balanced nanocluster formation reaction to formulate equations that can calculate transition-metal nanocluster size vs their formation time. Nor is there any mechanism-based treatment which deals with the important topic

Scheme 1

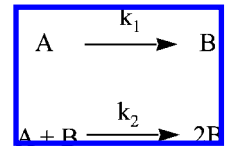

of the critical nucleus size,[15−17] nor as we define and use it herein, the catalytically effective nucleus. The main reason for this void is clear: until 1997 there were no detailed kinetic and mechanistic studies of transition-metal nanocluster formation that (a) started with a balanced nanocluster formation reaction, (b) yielded compositionally well-characterized nanoclusters, and which (c) included discrete mechanistic steps and rate constants that are the hallmarks of rigorous mechanistic studies (i.e., rather than just word statements of the "mechanism" which, of course, cannot be used to quantitatively fit kinetic data).[12]

The Finke−Watzky Two-Step Mechanism of Transition-Metal Nanocluster Formation. The 1997 Finke−Watzky (hereafter F−W) two-step mechanism for transition-metal nanocluster formation from metal salts under reductive conditions, such as H_2, is shown in Scheme 1,[12] in which A represents a reducible organometallic or inorganic precursor to the final nanoclusters and B represents the growing surface of the (e.g., Ir^0) nanocluster (Figure 1a).

The rate constants k_1 and k_2 for nucleation and autocatalytic growth, respectively, are determined via the established pseudoelementary step method using cyclohexene hydrogenation as a fast catalytic reporter reaction, eq 1,[18] where the factor of 1200 in eqs 1c and 1d is just the experimentally chosen ratio of cyclohexene to nanocluster precursor, A. The established, balanced reaction stoichiometry and a typical resulting, "S"-shaped sigmoidal kinetic curve for the prototype Ir^0 nanocluster system are shown in a and b of Figure 1, respectively. The sigmoidal curve consists of a flat, initial induction period during which nucleation is generally believed to occur. It has been experimentally demonstrated elsewhere[12] that k_1 is inversely proportional to the length of the induction period, i.e., k_1 (units: time^{-1}) ∝ $1/t_{induction}$ (units: time^{-1}).

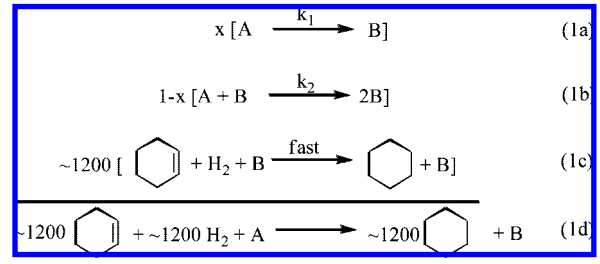

The induction period is then followed by fast autocatalytic reduction of the precursor A onto the nanocluster surface B. Also shown elsewhere[12] is that k_2 at constant $[A]_0$ (and more generally $k_2 \times [A]_0$[19]) is directly proportional to the normalized slope of the linear part of the curve after the induction period,

(8) Although nanocluster size control using seed clusters is well established, this method presumes the availability of small seeds of controlled size, narrow size dispersion, and known composition, something that is more rare. Buhro and co-workers have cleverly used $Au_{\sim 101}(PPh_3)_{21}Cl_5$ as seeds for Bi, In, and Sn nanoclusters with excellent results in size-dispersion control.[8b] Sau et al. used small gold nanoclusters as seeds for larger Au clusters;[8c] the sizes of the UV irradiation prepared seeds were controlled by the amount of reductant and nanocluster stabilizing ligand. Murphy et al. has examined the effects of rate of monomer addition to seeds on the growth of Au clusters on those seeds.[8d] Other examples of the seed method are available in the literature (e.g., see the refs summarized in the following references). (b) Yu, H.; Gibbons, P. C.; Kelton, K. F.; Buhro, W. E. *J. Am. Chem. Soc.* **2001**, *123*, 9198. (c) Sau, T. K.; Pal, A.; Jana, N. R.; Wang, Z. L.; Pal, T. *J. Nanopart. Res.* **2001**, *3*, 257. (d) Jana, N. R.; Gearheart, L.; Murphy, C. J. *Chem. Mater.* **2001**, *13*, 2313.
(9) Watzky, M. A.; Finke, R. G. *Chem. Mater.* **1997**, *9*, 3083.
(10) Hiramatsu, H.; Osterloh, F. E. *Chem. Mater.* **2004**, *16*, 2509.
(11) Kumar, S.; Gandhi, K. S.; Kumar, R. *Ind. Eng. Chem. Rev.* **2007**, *46*, 3128.
(12) Watzky, M. A.; Finke, R. G. *J. Am. Chem. Soc.* **1997**, *119*, 10382.
(13) Dixit, N. M.; Zukoski, C. F. *Phys. Rev. E* **2002**, *66*, 051602.
(14) Ji, X.; Song, X.; Li, J.; Yang, W.; Peng, X. *J. Am. Chem. Soc.* **2007**, *129*, 13939.
(15) Volmer, M.; Weber, A. *Z. Phys. Chem. (Leipzig)* **1926**, *119*, 227.
(16) Volmer, M. *Kinetik der Phasenbildung* (Kinetics of Phase Formation); Steinfopff: Leipzig, 1939.
(17) Becker, R.; Döring, W. *Ann. Phys.* **1935**, *24*, 719.
(18) Lin, Y.; Finke, R. G. *J. Am. Chem. Soc.* **1994**, *116*, 8335.
(19) Watzky, M. A; Ott, L. S.; Finney, E. E.; Finke, R. G. Transition-Metal Nanocluster Nucleation Kinetic and Mechanistic Studies, manuscript in preparation.

that is, $k_2 \times [A]_0$ (units: time^{-1}) $\propto$ slope/$[A]_0$ (units: time^{-1}), where $[A]_0$ represents the initial concentration of precursor A.

Overall, the mechanism in Scheme 1 is the simplest kinetic model that has proven able to fit a wide body of nanocluster nucleation and growth kinetic data[9,12,20] (i.e., an "Ockham's razor"[21] treatment, Ockham's razor being a basic tenant of rigorous mechanistic science). In more recent work, two additional steps have been discovered that occur following nanocluster formation, the steps of nanocluster bimolecular agglomeration (B + B $\rightarrow$ C, rate constant k_3)[22] and autocatalytic agglomeration (B + B $\rightarrow$ 1.5C, rate constant k_4).[23–25]

Since the self-assembly reaction that we call nanocluster formation necessarily consists of many steps, for example at least 300 (and probably more like 1000 or more) even for the formation of a "simple" $Ir_{\sim 300}$ nanocluster as shown back in Figure 1, some simplification and assumptions are necessary to obtain k_1 and k_2 from the kinetic data such as that shown in Figure 1. These simplifications and underlying assumptions, while already detailed in our prior papers,[12,20,24] are briefly summarized in the Supporting Information for the convenience of the interested reader. The assumption most relevant to the treatment of size vs time herein is that k_1 and k_2 are assumed to be independent of size. That is, *average* k_1 and an *average* k_2 rate constants are obtained from the curve-fits, such as that shown in Figure 1, and are then employed in the nanocluster size vs time equations which follow.

With a bit of reflection, one realizes that the size of the nanoclusters will depend on how many nuclei form, when nucleation effectively stops, and when growth begins (i.e., in the case where nucleation and growth are largely separated in time, *vide infra*, as desired for nanoclusters with a narrow size dispersion). Noteworthy here is that the induction time (i.e., the $k_1 \propto 1/t_{ind}$) and the fast downturn (i.e., $k_2 \times [A]_0 \propto$ slope/$[A]_0$) seen in Figure 1 is generally consistent with a separation in time of nucleation and growth. Further reflection makes it clear that nanocluster size should be related to the rate constants k_1 and k_2, as well as the initial metal concentration $[A]_0$, that is, when $k_2[A]_0/k_1$ is large, relatively few nuclei grow quickly into larger nanoclusters, whereas when $k_2[A]_0/k_1$ is small, more nuclei are being formed that are growing relatively slowly so that smaller nanoclusters are expected. Initial evidence that the $k_2[A]_0/k_1$ ratio correlates at least somewhat with nanocluster size was published in 1997.[9] In what follows, we will therefore also look at the limits of the nanocluster diameter vs time, D_t, equation in the two limits of $k_2[A]_0/k_1 \gg 1$ and $k_2[A]_0/k_1 \ll 1$.

The Focus of the Present Contribution: the Dependence of Nanocluster Size on k_1, k_2, $[A]_0$ and N^*, the Number of Atoms in the Catalytically Effective Nucleus. Herein we (i) show that the F−W two-step mechanism for nanocluster nucleation followed by autocatalytic growth can be used to provide an equation predicting nanocluster size vs time in terms of k_1, k_2, and $[A]_0$, and if the final size of the nanoclusters is known by, say, transmission electron microscopy (TEM) or other means. Also discussed is why it is not possible yet to predict the size vs time *ab initio* and unless either the final size, D_f, or the number of nuclei formed are known. However, we also (ii) show that with the assumption of a complete separation of nucleation and growth in time, the nanocluster size (D_t) vs time equation can be expressed in terms of the known k_1, k_2, $[A]_0$, and the final nanocluster size (D_f). We then (iii) obtain and present experimental TEM vs size data and show that this experimental data can be fit by, and thus conforms to, the D_t equation that is derived. We also (iv) use other TEM final size vs time data to calculate the catalytically effective nucleus number, N^*, for nine other Ir^0 nanocluster nucleation and growth systems previously examined in our laboratories. We furthermore (v) examine the limiting cases of very low and very high $[A]_0$, as well as the resulting $k_1 \gg k_2[A]_0$ and $k_1 \ll k_2[A]_0$. Finally, we (vi) summarize the known experimental variables that influence k_1 and k_2, and, therefore, also control nanocluster size, and we (viii) list some needed additional experiments and studies. Overall, this is the first contribution that treats the important and timely topic of nanocluster size control, and the related topic of the number of atoms in the catalytically effective nucleus (and, therefore, that nucleus' corresponding size) via a kinetically documented nanocluster formation mechanism.

Experimental Section

General Considerations. All manipulations were carried out under air-free conditions using a Vacuum Atmospheres N_2 drybox maintained at $\leq$5 ppm O_2 as monitored by a Vacuum Atmospheres O_2-level monitor. Unless indicated otherwise, all commercially available solvents, compounds and materials were used as received. Acetone (Burdick and Jackson, water content <0.2%) was purged with argon for 20 min and stored in the drybox. Cyclohexene (Aldrich, 99%) was purified by distillation over sodium under argon followed by storage in the drybox. Hydrogen gas (General Air, 99.5%) was purified by passing through a moisture trap, an O_2 cartridge, and an indicating O_2 trap (Trigon Technologies, Rancho Cordova, CA). The polyoxoanion-supported iridium nanocluster precursor complex $[Bu_4N]_5Na_3[(1,5\text{-COD})Ir\cdot P_2W_{15}Nb_3O_{62}]$ was prepared as previously described.[26]

The hydrogenation reaction was performed as previously described using our custom-built pressurized hydrogenation apparatus.[18] Briefly, 40 mg (7.2 μmol) of $[Bu_4N]_5Na_3[(1,5\text{-COD})Ir\cdot P_2W_{15}Nb_3O_{62}]$ was added to a 1-dram glass vial. Proton Sponge (1.6 mg, one equiv) was added to the vial. The solids were dissolved in 5.0 mL of acetone to make a clear, bright-yellow solution. This solution was added to a new 22 mm $\times$ 175 mm Pyrex borosilicate culture tube containing a new 5/8 in. $\times$ 5/16 in. Teflon-coated magnetic stir bar, and 1.0 mL of cyclohexene was added to the solution. The culture tube was placed in a Fischer−Porter (hereafter F−P) bottle, which was then sealed and brought out of the drybox. The bottle was placed in a mineral oil bath maintained at 22.0 $\pm$ 0.1 °C by a constant temperature recirculating water bath (VWR Scientific). The bottle was connected to the hydrogenation apparatus via its TFE-sealed Swagelock quick-connects. Stirring was started, and the bottle was purged 13 times with hydrogen (15 s per purge) and stirred for an additional 1 min 45 s (total time elapsed 5 min). The pressure in the bottle was set to 40.0 $\pm$ 0.1 psig H_2, $t = 0$ was noted, and data collection was initiated using an Omega PX-621 pressure transducer interfaced with a PC running LabVIEW 6.1.[18]

Kinetic Data/Curve-Fitting Analysis. Curve-fitting of the H_2 pressure loss (or, equivalently, by the 1:1 hydrogen:cyclohexene

(20) (a) Ott, L. S.; Finke, R. G. *Inorg. Chem.* **2006**, *45*, 8382. (b) Özkar, S.; Finke, R. G. *J. Am. Chem. Soc.* **2005**, *127*, 4800. (c) Özkar, S.; Finke, R. G. *Langmuir* **2003**, *19*, 6247. (d) Widegren, J. A.; Finke, R. G. *Inorg. Chem.* **2002**, *41*, 1558. (e) Weddle, K. S.; Aiken, J. D., III; Finke, R. G. *J. Am. Chem. Soc.* **1998**, *120*, 5653.
(21) Hoffmann, R.; Minkin, V. I.; Carpenter, B. K. *Int. J. Philos. Chem.* **1997**, *3*, 3.
(22) (a) Hornstein, B. J.; Finke, R. G. *Chem. Mater.* **2004**, *16*, 139. (b) See also the addition/correction in: Hornstein, B. J.; Finke, R. G. *Chem. Mater.* **2004**, *16*, 3972.
(23) Besson, C.; Finney, E. E.; Finke, R. G. *J. Am. Chem. Soc.* **2005**, *127*, 8179.
(24) Besson, C.; Finney, E. E.; Finke, R. G. *Chem. Mater.* **2005**, *17*, 4925.
(25) Finney, E. E.; Finke, R. G. *Chem. Mater.* **2008**, *20*, 1956.
(26) Pohl, M.; Lyon, D. K.; Mizuno, N.; Nomiya, K.; Finke, R. G. *Inorg. Chem.* **1995**, *34*, 1413.

stoichiometry, the cyclohexene loss) vs time data was performed, as described previously in detail,[27] by use of the software package Microcal Origin 7.0, a nonlinear regression subroutine (RLIN) which uses a modified Levenberg−Marquardt algorithm.[28] As before,[27] in the uncorrected H_2 pressure vs time curves one observes an initial small *increase* in the pressure due to the equilibration of the acetone solvent's vapor pressure after the F−P bottle is flushed with H_2 (15 times, 15 s/purge) and before the hydrogenation has started. This vapor pressure increase has been removed (as it should be) from the data used to generate, for example, Figure 1 as well as from all the other H_2 pressure vs time data used in this paper. This correction was accomplished as before[27] via a control experiment in which the acetone vapor pressure curve is measured independently for our apparatus followed by a point-by-point correction of the H_2 pressure loss data.

Removal of Samples for TEM Analysis. Samples for TEM size vs time were taken using the following procedure. First, the gas-regulator valve between the F−P bottle and the hydrogen tank was opened. Next, the top valve of the F−P bottle was opened to allow a continuous stream of H_2 through the F−P bottle and out of the top valve. A ~0.1 mL aliquot of the reaction solution was removed with a gastight syringe equipped with a 30 cm long needle, and the aliquot was placed in a 1 mL screwcap vial. The top valve of the F−P bottle was immediately closed. After waiting 10 s for the F−P bottle to become repressurized to ~40 psig of H_2, the valve to the hydrogen tank was closed. The entire operation took less than 1 min. The samples were prepared for TEM analysis by taking them to dryness immediately after removing them, and sending them to Clemson University where TEM images were obtained with the expert assistance of Dr. JoAn Hudson and her associates. The solid was dissolved in acetonitrile and placed on a grid (silicon monoxide type-A, Formvar backing, 300 mesh, copper grids, Ted Pella, Inc.).

Error Estimation in $[A]_t$ and N^*. As eq 15 was used to express $[A]_t$ in terms of $[A]_0$, D_t and D_f, we calculated the error bars in $[A]_t$ by propagating the experimental errors in D_t and D_f (reported at 1σ precision) using the proper procedure for propagating error rigorously in a function of several variables.[29] In the same manner, as eq 20 was used to express N^* in terms of k_1, k_2, $[A]_0$, t_{ind}, and D_f, we calculated the error bars in $[A]_t$ and N^* by propagating the experimental errors in k_1, k_2, t_{ind}, and D_f (reported at 1σ precision) using the same rigorous procedure.[29] The mathematical software MAPLE 11.0 was used to perform partial differentiations as well as calculations; details of the error propagation procedure are provided in the Supporting Information.

Note that the resultant error bars quoted for D_t and N^* in the text which follows are not derived from the distribution of nanocluster sizes that result experimentally from nucleation occurring over a period of time (i.e., and which one could treat by different k_1 "rate constants" as a function of time, so-called dispersive kinetics[30] rather than the use of a average, constant k_1 and k_2 as in this treatment, *vide infra*). The topic of nanocluster size distributions (i.e., and the dependence of nanocluster properties on that size distribution)[6–8,10,11,31] is an important, but different, problem that will need to be the topic of a separate treatment and paper.

Results and Discussion

1. Derivation of the Relation between Nanocluster Formation Kinetics and Nanocluster Size for a Spherical Nanocluster. Assuming a spherical nanocluster, as is experimentally observed for the Ir(0) and other nanoclusters we have made to date,[12,20,24] the volume, V, of a nanocluster with diameter D is given by eq 2:

$$V = \frac{4}{3}\pi\left(\frac{D}{2}\right)^3 = \frac{\pi D^3}{6} \tag{2}$$

The number of atoms in a nanocluster, defined as N, is then given by eq 3:

$$N = \frac{V\rho N_A}{MW} = \frac{\pi D^3 \rho N_A}{6MW} \tag{3}$$

Here, ρ is the density of the *bulk* metal, MW is its molecular weight, and N_A is Avogadro's number. (Use of the known bulk metal density in place of the unknown, expected to be slightly higher *nanocluster metal density* will result in a slight overestimate of the diameters, *vide infra*.)

Alternatively, solving for the diameter D gives eq 4:

$$D = \left(\frac{6NMW}{\pi\rho N_A}\right)^{\frac{1}{3}} \tag{4}$$

The number of atoms in each nanocluster at a given time, N_t, can also be given in terms of the total number of atoms incorporated into nanoclusters expressed relative to the total number of nanoclusters, as shown in eq 5a where it is assumed that the nanoclusters are *monodisperse* in size. The total number of atoms incorporated into nanoclusters may also be viewed as the total number of atoms in a hypothetical single nanocluster, as detailed in the section below.

$$N_t = \frac{\text{number of atoms incorporated into nanoclusters}}{\text{number of nanoclusters}} \tag{5a}$$

The number of atoms incorporated into nanoclusters can now be expressed in terms of the concentration of metal incorporated into nanoclusters at a given time, $[B]_t$, see eq 5b:

$$N_t = \frac{[B]_t V_{soln} N_A}{\text{number of nanoclusters}} \tag{5b}$$

For a clean reaction, A → B, the following is also true by mass balance, eq 5c,

$$[B]_t = [A]_0 - [A]_t \tag{5c}$$

so that eq 5d results:

$$N_t = \frac{([A]_0 - [A]_t)V_{soln} N_A}{\text{number of nanoclusters}} \tag{5d}$$

In eqs 5a−d, $[A]_0$ is the initial metal nanocluster precursor concentration, $[A]_t$ is the concentration of the precursor at time t, and V_{soln} is the volume of the solution.

(27) Widegren, J. A.; Aiken, J. D., III; Özkar, S.; Finke, R. G. *Chem. Mater.* **2001**, *12*, 312.
(28) Press, W. H.; Flannery, B. P.; Teukolsky, S. A.; Vetterling, W. T. *Numerical Recipes*; Cambridge University: Cambridge, U.K., 1989.
(29) (a) Bevington, P. R.; RobinsonD. K. *Data Reduction and Error Analysis for the Physical Sciences*, 2nd ed.; McGraw-Hill: New York, 1992; pp 41−50; (b) Andraos, J. *J. Chem. Educ.* **1996**, *73*, 150–154.
(30) Plonka, A. *Annu. Rep. Prog. Chem., Sect. C: Phys. Chem.* **2001**, *97*, 91.
(31) Finke, R. G. In *Metal Nanoparticles: Synthesis, Characterization, and Applications*; Feldheim, D. L.; Foss, C. A., Jr., Eds.; Marcel Dekker: New York, 2002; Chapter 2.

Table 1. Kinetic Data and Final Nanocluster Size by TEM for Nine Different Ir Nanocluster Systems along with the Computed N^*.[a]

entry	precursor	t_{ind}, h	k_1, h^{-1}	$k_2 \times 10^{-3}$, $M^{-1}\cdot h^{-1}$	$k_2/k_1 \times 10^{-4}$, M^{-1}	d, nm (TEM)	average N^* from eq 20[b,c]	N^* range (size, nm)
1	$[Ir(1,5\text{-COD})(CH_3CN)_2][BF_4]$ + $[Bu_4N]_9[P_2W_{15}Nb_3O_{62}]$	1.5(3)	0.008(1)	1.5(1)	19(2)	2.1(4)	20(16)	4−36(0.5−1)
2[40b]	$[Bu_4N]_5Na_3[(1,5\text{-COD})Ir\cdot P_2W_{15}Nb_3O_{62}]$	1.0(2)	0.015(1)	2.8(1)	19(1)	2.2(3)	44(33)	11−77(0.7−1.3)
3	$[Bu_4N]_5Na_3[(1,5\text{-COD})Ir\cdot P_2W_{15}Nb_3O_{62}]$ + 1 equiv Proton Sponge	0.7(1)	0.008(1)	3.5(1)	44(5)	2.1(4)	11(8)	3−19(0.4−0.8)
4	$[Bu_4N]_4Na_2[(1,5\text{-COD})Ir\cdot SiW_9Nb_3O_{40}]$	0.5(1)	0.049(3)	3.7(1)	7.6(5)	2.2(4)	33(24)	9−57(0.6−1.1)
5	$[Bu_4N]_4Na_2[(1,5\text{-COD})Ir\cdot SiW_9Nb_3O_{40}]$ + 1 equivalent Proton Sponge	0.5(1)	0.040(2)	4.7(1)	12(1)	2.1(4)	35(28)	7−63(0.6−1.2)
6	$[Ir(1,5\text{-COD})(CH_3CN)_2][BF_4]$ + $[Bu_4N]_{(8n+1)}[P_2W_{15}(TiOH)_3O_{59}]_n$	0.7(2)	0.021(2)	4.1(1)	20(1)	2.2(3)	46(46)	0−92(0−1.4)
7	$[Ir(1,5\text{-COD})(CH_3CN)_2][BF_4]$ + $[Bu_4N]_{(8n+1)}[P_2W_{15}(TiOH)_3O_{59}]_n$ + 1 equiv Proton Sponge	1.0(2)	0.009(1)	2.8(1)	31(3)	2.1(3)	24(19)	5−43(0.5−1.0)
8	$[Ir(1,5\text{-COD})(CH_3CN)_2][BF_4]$ + $[Bu_4N]_3C_6H_5O_7$	2.0(2)	0.022(2)	1.1(1)	5.0(5)	2.3(5)	83(59)	24−142(0.9−1.6)
9	$[Ir(1,5\text{-COD})(CH_3CN)_2][BF_4]$ + $[Bu_4N]_3C_6H_5O_7$ + 1 equiv Proton Sponge	1.2(2)	0.015(1)	2.0(1)	13(1)	1.8(4)	21(17)	4−38(0.5−1.0)

[a] Full experimental details for the data in this table have been published,[40] and the data for this table are all taken from a 2002 paper.[40] The initial concentration in each reaction is 1.2 mM in 2.5 mL of acetone and 0.5 mL of cyclohexene.[40] [b] The following values were used in eq 20: $\rho(Ir) = 22.65$ g/cm^3; MW(Ir) = 192.22 g/mol; $[A]_0 = 1.2$ mM; $V_{soln} = 3.0$ mL. [c] The error bars for N^* shown were propagated rigorously, as described in the Experimental Section and elsewhere,[29] from the uncertainties in t_{ind}, k_1, and k_2, as well as the standard deviations for the sizes of the nanoclusters.

Solving for the number of nanoclusters gives eq 6:

$$\text{number of nanoclusters} = \frac{([A]_0 - [A]_t)V_{soln}N_A}{N_t} \quad (6)$$

2. Relation between Nanocluster Formation Kinetics and Nanocluster Size in a Hypothetical Single Nanocluster. If we go back to eq 5d and set the unknown value for the total number of nanoclusters equal to one, so that the atoms incorporated into nanoclusters become one hypothetical single nanocluster, we obtain eq 7a for the number of atoms in that hypothetical single nanocluster as a function of time:

$$N_{single(t)} = ([A]_0 - [A]_t)V_{soln}N_A \quad (7a)$$

Subsequently, we can substitute eq 7a into eq 4 to express the diameter of a hypothetical single nanocluster, eq 7b

$$D_{single(t)} = \left(([A]_0 - [A]_t)\frac{6MWV_{soln}}{\pi\rho}\right)^{\frac{1}{3}} \quad (7b)$$

We can express $[A]_t$ in terms of $[A]_0$, k_1, and k_2 using the integrated rate equation corresponding to the two-step mechanism in Scheme 1, eq 8: [12]

$$[A]_t = [A]_0 \times \frac{k_1 + k_2[A]_0}{k_2[A]_0 + k_1 \times e^{(k_1+k_2[A]_0)t}} \quad (8)$$

Use of the integrated eq 8 into eq 7 leads to the expression in eq 9.

$$D_{single(t)} = \left([A]_0\left(1 - \frac{k_1 + k_2[A]_0}{k_2[A]_0 + k_1 \times e^{(k_1+k_2[A]_0)t}}\right)\frac{6MWV_{soln}}{\pi\rho}\right)^{\frac{1}{3}} \quad (9)$$

To obtain a graphic feel for eq 9, a numerical simulation was carried out (i.e., by assuming for the moment that all of the metal atoms go into a single nanocluster). Using typical values for k_1 and k_2 from entry 2 in Table 1 (*vide infra*) for Ir^0 nanoclusters prepared from $[(1,5\text{-COD})Ir\cdot P_2W_{15}Nb_3O_{62}]^{8-}$, along with our standard conditions of a 3.0 mL solution that is 1.2 mM Ir, eq 9 allows the generation of the size vs time curve[32] shown in Figure 2. A smooth progression to a hypothetical, "single nanocluster" of final diameter of $3.8(5) \times 10^5$ nm results.

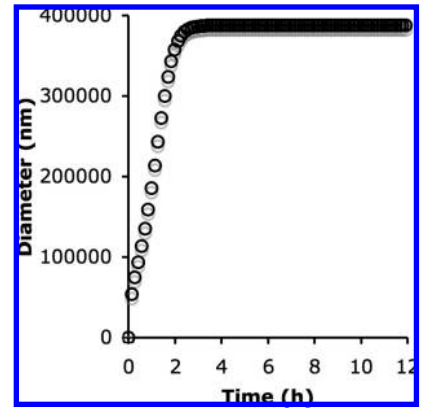

Figure 2. Simulation of the size vs time for the formation of a hypothetical "single Ir^0 nanocluster" and for the Ir^0 nanocluster formation reaction and conditions in entry 2 of Table 1. The final size is "$3.8(5) \times 10^5$ nm" in this simulation, one done primarily to obtain a feel for the shape of the size vs time curve as well as to illustrate the need for knowing the total number of nanoclusters formed. The following values were used in eq 9: $\rho(Ir) = 22.65$ g/cm^3; MW(Ir) = 192.22 g/mol; $[A]_0 = 1.2$ mM; $V_{soln} = 3.0$ mL.

3. Relation between Nanocluster Formation Kinetics and Nanocluster Size When the Final Nanocluster Size Is Known. If we assume that nucleation and growth are completely separated in time, then the nuclei are finished forming by the end of the induction period, and growth then occurs via the subsequent addition of atoms onto the existing nuclei. In this case, the number of nanoclusters at any time past the end of the induction period is equal to the number of catalytically effective nuclei formed (*vide infra*). Therefore, we assume

(32) (a) Interestingly, size vs time curves similar to Figure 2 have been observed in the flocculation of activated sludge. In that case, population balance modeling of sludge particles, using mathematical formulas to describe floc formation via aggregation and destruction by breaking, was used to describe the flocculation process.[32b] (b) Ding, A.; Hounslow, M. J.; Biggs, C. A. *Chem. Eng. Sci.* **2006**, *61*, 63.

thereafter that the number of nanoclusters in eq 6 remains *constant* after the end of the induction period.

If the final nanocluster size, D_f, is known (*vide infra*), then the final number of atoms in a nanocluster, N_f, can be calculated from eq 3, as shown in eq 10, assuming again that the nanoclusters' size is monodisperse.

$$N_f = \frac{\pi D_f^3 \rho N_A}{6MW} \tag{10}$$

Equation 6 can then be expressed at *the end of the reaction* (at $t = t_f$,), to give eq 11a where it is assumed that all A precursor is consumed in the reaction (i.e., that $[A]_f = 0$).

$$\text{number of nanoclusters} = \frac{[A]_0 V_{soln} N_A}{N_f} \tag{11a}$$

Substitution of N_f with eq 10 gives eq 11b:

$$\text{number of nanoclusters} = \frac{[A]_0 V_{soln} 6\ MW}{\pi D_f^3 \rho} \tag{11b}$$

An expression for the (average) number of atoms in a nanocluster as a function of time, N_t, is now obtained by substituting eq 11b for the number of nanoclusters into eq 5d above, see eq 12, where as before N_A is Avogadro's number:

$$(\text{at } t \geq t_{ind})\ \ N_t = \frac{D_f^3 \pi \rho N_A}{6MW}\left(\frac{[A]_0 - [A]_t}{[A]_0}\right) \tag{12}$$

Alternatively, eq 4 can be used along with eq 12 to express instead the nanocluster diameter as a function of time, D_t, as shown in eq 13 below.

$$(\text{at } t \geq t_{ind})\ \ D_t = D_f\left(\frac{[A]_0 - [A]_t}{[A]_0}\right)^{\frac{1}{3}} \tag{13}$$

In other words, *the size of the nanoclusters at time t is simply the fraction of the concentration of nanoclusters at time t, $[B]_t/[A]_0$ (or alternatively, $([A]_0 - [A]_t)/[A]_0$) to the 1/3 power, multiplied by the final diameter*. This gives a very simple equation[33] for determining D_t if the final size is known from TEM, SAXS, EXAFS, or other measurements. If we know $[A]_t$ (from following the hydrogenation of cyclohexene) and, therefore, $[B]_t$, we can therefore use eq 13 to convert that concentration vs time data to size vs time data once the final size D_f is known.

Substituting the integrated rate eq 8 from the F−W mechanism in Scheme 1[12] into eq 13, gives eq 14 which is an expression for D_t in terms of quantities that can be obtained either in a handbook or by experiment.

$$(\text{at } t \geq t_{ind})\ \ D_t = D_f \times \left(1 - \frac{k_1 + k_2[A]_0}{k_2[A]_0 + k_1 \times e^{(k_1 + k_2[A]_0)t}}\right)^{\frac{1}{3}} \tag{14}$$

A reminder summarizing the approximations and assumptions that have gone into deriving eq 14 is provided in a footnote.[34]

4. Example of the Relation between Nanocluster Formation Kinetics and Nanocluster Size When the Final Nanocluster Size Is Known: Experimental Data Showing the Growth of $Ir_{\sim 300}$ Nanoclusters over Time. We followed the reduction of 1.2 mM $[Bu_4N]_5Na_3[(1,5\text{-COD})Ir{\cdot}P_2W_{15}Nb_3O_{62}$ under H_2 to yield Ir^0 nanoclusters, and removed samples for TEM analysis at eight different times from 0.5 to 40 h, Figure 3a, to see how the size of the nanoclusters changes over time. That experimental size vs time data was then compared to the calculated size vs time data using eq 14 to provide evidence

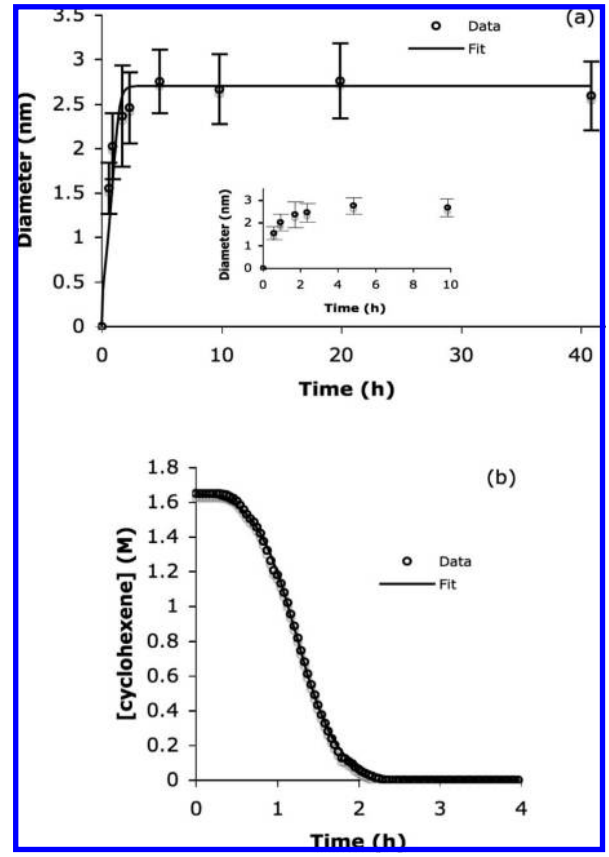

Figure 3. (a) Ir^0 nanocluster size vs time from TEM images collected over the course of a reduction of $[Bu_4N]_5Na_3[(1,5\text{-COD})Ir{\cdot}P_2W_{15}Nb_3O_{62}]$ (the inset shows the early time data over the first 10 h), and (b) the associated cyclohexene hydrogenation reporter reaction kinetic curve for that same nanocluster formation reaction. The fit in (b) is to the two-step F−W mechanism for nucleation and autocatalytic growth, A → B, A + B → 2B: $k_1 = 0.028(2)\ h^{-1}$, $k_2 = 3.37(9) \times 10^3\ M^{-1}\ h^{-1}$. The curve fit in (a) is to eq 14 using these measured k_1, k_2, the final diameter $D_f = 2.7$ nm, and the known $[A]_0 = 0.0012$ M. The induction period in (b) is 0.42 h. Also, the value of N^* (eq 20, *vide infra*) calculated from curve fitting (b) is $N^* = 22$.

(33) (a) Interestingly, a related (but empirically-based) treatment exists in the work of Turkevich;[33b] further investigation into that work will be reported in due course. (b) Turkevich, J.; Stevenson, P. C.; Hillier, J. *Discuss. Faraday Soc.* **1951**, *11*, 55.

(34) The approximations and definitions used to obtain eq 14, and hence the equations which follow it, are: (i) that the two-step mechanism operates and closely fits the data (i.e., so that no agglomeration steps are present as is the case in the four-step mechanism for transition-metal nucleation, growth *and two types of agglomeration*, Scheme S1 of the Supporting Information); (ii) that nucleation and growth are effectively separated in time, so that the number of nuclei remains constant after the end of the induction period; (iii) that the nanoclusters are monodisperse in size (this is in part a restatement of (ii)); (iv) that the bulk-metal density, ρ, is a reasonable approximation to the actual density of the nanocluster; and (v) that N^* (*vide infra)* is the number of atoms in the catalytically effective nucleus as defined and used herein. The approximations underlying the two-step treatment of the kinetic data, and extraction of two (average) k_1 and k_2 rate constants, are also built into the present treatment and as summarized in the Supporting Information section on "Simplifications and assumptions underling the Finke−Watzky mechanism for transition-metal nanocluster nucleation and growth".

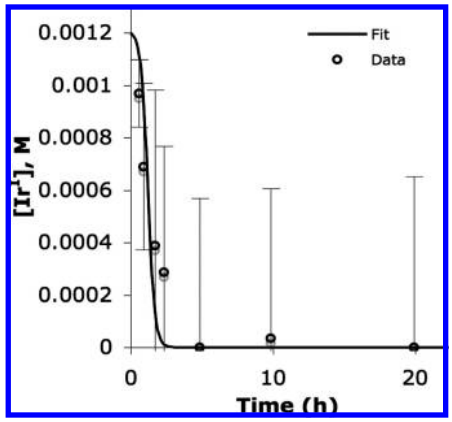

Figure 4. Ir^I concentration vs time data derived using eq 15 with the nanocluster TEM size data from Figure 3a ("data"), and calculated using eq 8 with the k_1 and k_2 values extracted from the curve-fit of cyclohexene loss in Figure 3b ("fit"). The first data point is after the end of the induction period ($t = 0.58$ h).

for the validity of eq 14. The associated cyclohexene hydrogenation kinetic curve observed is shown in Figure 3b. A representative TEM image and distribution histogram from each measurement is provided in the Supporting Information.

The first observation is that even though TEM sampling vs time provides a limited amount of lower precision size data vs time, *the general shape of the predicted curve in Figure 2* and of the observed data points in Figure 3a are similar (see the insert in Figure 3a as well), semiquantitative verification of the size vs time treatment leading up to eq 14 which in turn was used to generate Figure 2. Remember that before the end of the induction period, the number of nuclei is still increasing with time, so that eq 14 becomes valid only at the end of the induction period and thereafter.

Moving back one equation, a specific example of going from size to concentration data using eq 13 is of interest, and so we illustrate this using the size vs time data collected in Figure 3a. We can convert eq 13 into an expression for [A] vs time, using the known value of $[A]_0$ and the measured values of D_t and D_f from TEMs (see Figure 3a), as shown in eq 15 below.

$$(\text{at } t \geq t_{\text{ind}}) \quad [A]_t = [A]_0\left(1 - \left(\frac{D_t}{D_f}\right)^3\right) \tag{15}$$

The plot of [A] vs time using the TEM diameters from Figure 3a is shown in Figure 4. The fit shown in Figure 4 is to the F−W two-step mechanism in eq 8 using the k_1 and k_2 rate constants which resulted from the cyclohexene loss data in Figure 3b. The large experimental error involved in the TEM-determined diameters is apparent, the reason being that $[A]_t$ is proportional to the third power of the diameter, D_t^3. The purpose of Figure 4 is just to show the correspondence of the data in Figure 3 and the alternative presentation of it in Figure 4, that is, the A_t and D_t connection made apparent via eq 15.

5. The Relation between Nanocluster Formation Kinetics and Nanocluster Size: the Need To Know the Number of Atoms in the Catalytically Effective Nucleus, *N.** Alternatively, we can choose to express eq 6 for the number of nanoclusters, at time $t = t_{\text{ind}}$ at the end of the induction period. The number of atoms in a nanocluster at $t = t_{\text{ind}}$ is proportional to what we define as *N**, the *number of atoms in the catalytically effective nucleus*, eq 16.

$$\text{number of nanoclusters} = \frac{([A]_0 - [A]_{t_{\text{ind}}})V_{\text{soln}}N_A}{N^*} \tag{16}$$

*N** is the number of atoms present in the *average* size nucleus at the end of the induction period and when H_2/cyclohexene loss (catalysis) begins to be observable (e.g., see Figure 1b or 3b); hence, the descriptive name the "catalytically effective nucleus". In eq 16, $[A]_{t(\text{ind})}$ represents the concentration of A at the end of the induction period, that is, when nanocluster nucleation is complete. Note that we make no claim at this point whether the so-called "critical nucleus" of classical nucleation theory[15–17] is the same as (or even related to) the "catalytically effective nucleus number" present at $t = t_{\text{ind}}$ as defined and used herein.

Substitution of eq 16 for the number of nanoclusters, into eq 5d for the number of atoms in a nanocluster as a function of time, provides a new expression for N_t in terms of *N**, eq 17 below. Here again, key assumptions are that nucleation and growth are separated in time, and that the nanoclusters' size is monodisperse (*vide supra*).

$$(\text{at } t \geq t_{\text{ind}}) \quad N_t = N^*\left(\frac{[A] - [A]_t}{[A]_0 - [A]_{t_{\text{ind}}}}\right) \tag{17}$$

Use of eq 4 provides an expression for the nanocluster size as a function of time, D_t, in terms of *N**, eq 18.

$$(\text{at } t \geq t_{\text{ind}}) \quad D_t = \left(\frac{N^*6\text{MW}}{\pi\rho N_A}\left(\frac{[A]_0 - [A]_t}{[A]_0 - [A]_{t_{\text{ind}}}}\right)\right)^{\frac{1}{3}} \tag{18}$$

Ideally, we could use the integrated rate eq 8 to express [A] as a function of time in eq 18, and thus to determine the size of the nanoclusters as a function of time with no size data already in hand (i.e., using only observed or measured values of k_1, k_2, $[A]_0$, and t_{ind}). Unfortunately, this cannot presently be done because the number of atoms in the catalytically effective nucleus cannot at present be determined *ab initio* for such transition-metal nanoclusters in solution. The critical nucleus size is itself dependent on the kinetics of nanocluster formation, which determine when nanocluster nucleation stops and growth begins. The exact nature of this dependence is presently unknown.

In terms of classical nucleation theory and the (classical) critical nucleus, theoretical simulations are the most common means of estimating the number of atoms, and thus size, of the (classical) critical nucleus, but those treatments *are strictly valid only for gas-to-liquid nucleation*.[35] Calculations of (classical) critical nuclei have been performed for freezing (using experimental differential scanning calorimetry data)[36] and metal cluster formation in microemulsions (using computer simulations).[37] While some theoretical work has appeared for transition-metal nanoclusters,[38] conclusive results have not been obtained.[39] Moreover, because the at least classical critical nucleus is, by definition, the least stable species en route to nanocluster

(35) See for example:(a) Zachariah, M. R.; Carrier, M. J. *J. Aerosol Sci.* **1999**, *30*, 1139. (b) Zachariah, M. R.; Carrier, M. J.; Blaisten-Bajoras, E. *J. Phys. Chem.* **1996**, *100*, 14856. (c) Hawa, T.; Zachariah, M. R. *Phys. Rev. B* **2004**, *69*, 035417−1.
(36) Liu, J.; Nicholson, C. E.; Cooper, S. J. *Langmuir* **2007**, *23*, 7286.
(37) Tojo, C.; Barroso, F.; de Dios, M. *J. Colloid Interface Sci.* **2006**, *296*, 591.
(38) (a) Ciacchi, L. C.; Pompe, W.; De Vita, A. *J. Am. Chem. Soc.* **2001**, *123*, 7371. (b) Ciacchi, L. C.; Pompe, W.; De Vita, A. *J. Phys. Chem. B* **2003**, *107*, 1755.
(39) Finney, E. E.; Finke, R. G. *J. Colloid Interface Sci.* **2008**, *317*, 351.

formation, its direct detection experimentally is expected to be extremely difficult. Quite simply, at present the number of atoms in the catalytically effective or classic critical nucleus cannot be readily determined, except perhaps via population balance modeling,[11] an approach under consideration. Therefore, in this first paper treating nanocluster size vs time via a documented mechanism, our approach is to use the experimentally determined nanocluster size to determine the value of N^*. The *ab initio* prediction of N^* for transition-metal nanoclusters in solution remains an unsolved problem.

6. Application of the Relation between Nanocluster Formation Kinetics and Nanocluster Size When the Final Nanocluster Size Is Known: Determination of the Catalytically Effectiive Nucleus Number, N^*. The number N^* can be obtained from eq 12 when the final nanocluster size is known, at time $t = t_{ind}$ as shown in eq 19 below.

$$N^* = \frac{D_f^3 \pi \rho N_A}{6MW}\left(\frac{[A]_0 - [A]_{t_{ind}}}{[A]_0}\right) \quad (19)$$

Use of the integrated rate eq 8 to express $[A]_t$ in terms of k_1, k_2, and $[A]_0$ gives eq 20 which we will use herein to calculate N^* in several transition metal nanocluster systems.

$$N^* = \frac{D_f^3 \pi \rho N_A}{6MW} \times \left(1 - \frac{k_1 + k_2[A]_0}{k_2[A]_0 + k_1 \times e^{(k_1 + k_2[A]_0)t_{ind}}}\right) \quad (20)$$

In order to emphasize which factors will determine the final size D_f, a simple rearrangement of eq 20 can be made to give eq 21 with D_f as a function of the variables N^*, k_1, k_2, $[A]_0$ and t_{ind}.

$$D_f = \left(\frac{N^* 6MW}{\pi \rho N_A} \times \left(\frac{1}{1 - \frac{k_1 + k_2[A]_0}{k_2[A]_0 + k_1 \times e^{(k_1 + k_2[A]_0)t_{ind}}}}\right)\right)^{\frac{1}{3}} \quad (21)$$

In the same manner, eq 11b can also be rearranged to yield eq 22 for the final size, D_f, via an equation that involves knowing $[A]_0$ and the number of nanoclusters.

$$D_f = \left(\frac{[A]_0 V_{soln} 6MW}{\pi \rho \times \text{number of nanoclusters}}\right)^{\frac{1}{3}} \quad (22)$$

In 2002, we reported a study of Ir^0 nanocluster formation using a variety of Ir^I precursor complexes, $(1,5\text{-COD})Ir^+/(\text{anion})^{n-}$.[40] Nine of these experiments are collected in Table 1, along with the kinetic data (t_{ind} and rate constants k_1 and k_2) and nanocluster size as determined by TEM in that study.[40] We can use the data in Table 1 along with eq 20 to calculate the values of N^* for those nine, related Ir nanocluster forming systems. We can therefore see how the value of N^* changes with k_1, k_2, and t_{ind} (and while noting that t_{ind} is itself dependent on k_1, k_2, and $[A]_0$). However, since $[A]_0$ is the same ($[A]_0 = 0.0012$ M) in each set of experiments in Table 1, the effects of $[A]_0$ on N^* as well as on final size will not be discernible from the data in Table 1. We also can use eq 20 along with the maximum and minimum sizes observed by TEM to obtain, respectively, the largest and smallest nuclei in each experiment. Those data are also collected in Table 1. The corresponding nucleus *size* can be readily calculated using eq 4; those values are also shown in Table 1. These are the first estimates of a catalytically effective nucleus number, and corresponding size, for a transition-metal nanocluster formation.

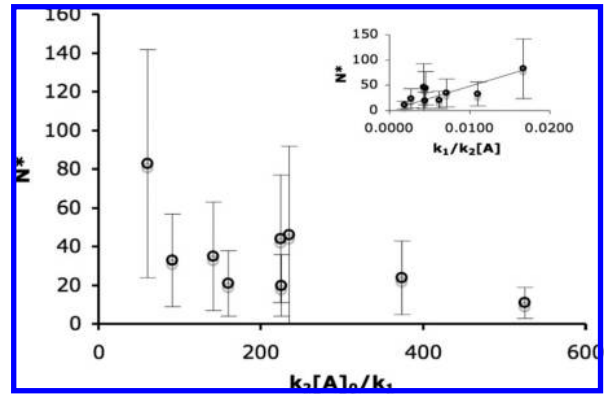

Figure 5. Plot of N^* vs $k_2[A]_0/k_1$. Although many of the values of N^* in the $k_2[A]_0/k_1 = 100-400$ region are not different beyond the rigorously propagated experimental error, the full data set reveals a general trend of decreasing N^* with increasing $k_2[A]_0/k_1$.

A couple of interesting results are immediately visible from Table 1. First, the nucleus number, N^*, at least as calculated according to the treatment herein, is between ca. 11(±8) to 83(±59) atoms, that is, within the general range of the first (13 atoms), second (55 atoms), and third (147 atoms) "magic number" size nanoclusters (really just full shell, and thus somewhat more stable, nanoclusters).[41] Second, the values of N^* computed according to eq 20 exhibit a range of a factor of ca. 2−8 fold, even given the sizable propagated errors, while the $k_2[A]_0/k_1$ ratio ranges about 2−9 fold. Interestingly, there is also a general *decrease* in N^* as the $k_2[A]_0/k_1$ ratio *increases*, Figure 5. This trend is verified by alternatively plotting N^* as a function of $k_1/k_2[A]_0$; note the expected value of $N^* = 0$ for $k_1 = 0$, and thus also for $k_1/k_2[A]_0 = 0$, matches the intercept of the N^* vs $k_1/k_2[A]_0$ plot within experimental error. The approximately linear relationship between N^* and $k_1/k_2[A]_0$ at the present precision of the data is shown as the insert in Figure 5.

The decrease in the number of atoms in the nucleus, N^*, and thus therefore also the decreasing size of the nucleus with increasing $k_2[A]_0/k_1$ makes sense: a larger $k_2[A]_0/k_1$ ratio means fewer, smaller nuclei followed by greater growth of those nuclei. But, in terms of the overall nanocluster size, these fewer, smaller catalytically effective nuclei have both more time and more A to consume, so that they grow to larger *final* sizes, at least when nucleation and growth are largely separated in time as the autocatalytic growth step tends to enforce. In short, the implication is that smaller nuclei lead to larger nanoclusters. Third, since the acetone solvent in these studies was also held constant, the change in the $k_2[A]_0/k_1$ ratio and nucleus size must be due to the primary difference between the entries in Table 1, *namely the different anionic ligands present* in the precursor of general formula $[(1,5\text{-COD})Ir^+]/(\text{anion})^{n-}$. It follows, then, that the catalytically effective nucleus number and corresponding size is being affected by the ligands that are present. Other factors also known to affect the kinetics of nanocluster formation will be summarized in an upcoming section.

A fourth, very noteworthy observation from the results summarized in Table 1 is that, at least for the closely related systems in Table 1 *and at the constant $[A]_0$ employed* while in the same solvent (acetone), the range of final nanocluster sizes

(40) (a) Özkar, S.; Finke, R. G. *Langmuir* **2002**, *18*, 7653. (b) Özkar, S.; Finke, R. G. *J. Am. Chem. Soc.* **2002**, *124*, 5796.
(41) Teo, B. K.; Sloane, N. J. A. *Inorg. Chem.* **1985**, *24*, 4545.

is relatively *insensitive* to the $k_2[A]_0/k_1$ ratio. In all of the experiments except entry 9, the nanocluster size is 2.1−2.3 nm. Even the diameter in entry 9 (1.8 nm) is within the standard deviation of the rest, while the ratio k_2/k_1 varies nearly 10-fold, from $5.0(6) \times 10^4$ M^{-1} to $44(6) \times 10^4$ M^{-1}. In short, for the closely related $[(1,5\text{-COD})Ir^+]^{n+}(anion)^{n-}$ systems and constant $[A]_0$ conditions listed in Table 1, the final size of the nanoclusters is largely insensitive to the $k_2[A]_0/k_1$ ratio. Our belief is that this is actually not in conflict with the initial implications and expectations, discussed above, for how nanocluster final size should vary with the $k_2[A]_0/k_1$ ratio as noted above. Rather, the insight and hypothesis for future research here is that a much larger $k_2[A]_0/k_1$ ratio to achieve good size control is needed than is present for the above, closely related systems. The *constant $[A]_0$ employed in these experiments is also implicated as a poor choice if one wishes to achieve better size control. Experiments using the largest possible experimental differences in $[A]_0$ are hereby suggested as worth trying to achieve better nanocluster size control.* The above, needed future experiments so noted, it is worth emphasizing that eq 18 and eq 8 teach that k_1, k_2, and $[A]_0$ are highly convoluted into D_t, the nanocluster size as a function of time. It follows, then and overall, that additional, systematic studies will be needed to flush out the precise, quantitative connection of final size with the $k_2[A]_0/k_1$ ratio and the connected issue of the nucleus number N^* as a function of $k_2[A]_0/k_1$. It will be important in these studies to examine a range of metals under a variety of anionic and other stabilizers, changing $[A]_0$, solvents and other reaction conditions.

7. Examination of the Limiting Cases of Very Low or Very High $[A]_0$, k_1 or k_2. It is instructive to observe how certain limiting cases affect the nanocluster size and nanocluster size vs time profile. Two limiting cases are apparent: very high and very low $[A]_0$ (i.e., the use of $[A]_0$ variations to achieve nanocluster size control), and the cases of very high and very low k_1 or k_2 (i.e., the use of k_1 and k_2 variations to achieve nanocluster size control).

In the case of very low $[A]_0$ (without any assumptions on the respective values of k_1 and k_2), we obtain $k_1 \gg k_2[A]_0$ so that eq 14 for the nanocluster size as a function of time simplifies to eq 23. Most notably, the growth rate constant k_2 (and $[A]_0$) fall out of the equation; this means that at low enough metal concentration, the nanocluster size becomes dependent mostly on k_1. This is an uncommon case in at least our experience, one where there would be little to no induction period so that it would likely be difficult if not impossible to verify if the two-step mechanism were present and, therefore, to ascertain if eq 23 even applied.

$$(\text{at } t \geq t_{\text{ind}}) \quad D_t = D_f(1 - e^{-k_1 t})^{\frac{1}{3}} \tag{23}$$

The limiting case of very high $[A]_0$ (again, without any assumptions on the respective values of k_1 and k_2), in which $k_1 \ll k_2[A]_0$, simplifies eq 14 to eq 24.

$$(\text{at } t \geq t_{\text{ind}}) \quad D_t = D_f\left(\frac{1}{1 + \frac{k_2[A]_0}{k_1} \times e^{-k_2[A]_0 t}}\right)^{\frac{1}{3}} \tag{24}$$

In the kinetic limiting case of very low k_1 (where $k_1 \ll k_2[A]_0$), we find that $D_t = 0$ from eq 14, not an especially interesting case. In another kinetic limiting case of either very high k_1, or very low k_2 (where $k_1 \gg k_2[A]_0$), eq 14 simplifies again to eq 23, the same as the limit of low $[A]_0$. In the last limiting case of very high k_2 (where $k_1 \ll k_2[A]_0$), eq 14 simplifies to eq 24, the same as the limit of high $[A]_0$. Experimental verification of at least the more interesting of these predicted limits is another important goal for future research.

8. Other Known Factors That Affect Nanocluster Formation Kinetics and, Therefore, Nanocluster Size. There are several factors that have been found to have an effect on the kinetics of nanocluster nucleation and growth, which the equations herein demonstrate will in turn influence the final size of the nanoclusters. Those that have been studied for the prototype $Ir(0)_n$ nanocluster system include ligands,[25] the reduction potential of the metal,[23–25] trace impurities in the solvents used such as water[12] or an intriguing, but still unidentified impurity in acetone solvent (see Figure G of the Supporting Information of ref 42), olefins such as cyclohexene (with cyclohexene $Ir_{\sim 300}$ nanoclusters are formed,[42] but without cyclohexene $Ir_{\sim 900}$ are formed[18]), small-molecular weight polymers,[43] and the rate of H_2 gas-to-solution mass transfer (i.e., with poor H_2 mass transfer, agglomerated, broadly dispersed, and considerable inferior nanoclusters result).[44] Interestingly, temperature appears to be less of a factor, at least for Ir^0 nanoclusters under the conditions employed to date, than one might have expected, again judging from the (limited) data presently available.[12,25] For example, the $P_2W_{15}Nb_3O_{62}^{9-}$ polyoxoanion-stabilized $Ir^0_{\sim 300}$ nanoclusters show activation parameters for the (average) k_1 and (average) k_2 steps in acetone that are rather similar, $\Delta H_1^{\ddagger} = 15(1)$ kcal/mol, $\Delta S_1^{\ddagger} = -36(3)$ eu and $\Delta H_2^{\ddagger} = 14(2)$ kcal/mol, $\Delta S_2^{\ddagger} = -13(6)$ eu (1 M standard state).[12] The implication is that, again at least for these specific systems and conditions used, temperature cannot easily be used to greatly favor the nucleation over the growth step. Similarly, Ir^0 nanoclusters stabilized by Cl^- in propylene carbonate solvent also show somewhat analogous activation parameters for the k_1 and k_2 steps in that system, $\Delta H_1^{\ddagger} = 15(1)$ kcal/mol, $\Delta S_1^{\ddagger} = -14(1)$ eu and $\Delta H_2^{\ddagger} = 10(2)$ kcal/mol, $\Delta S_2^{\ddagger} = -11(4)$ eu.[25] The caveat here is that these two systems are rather similar in many respects: H_2 as the reductant of a $Ir(1,5\text{-COD})^+$-based nanocluster precursor. The trend of smaller nanoclusters for metals with larger $\Delta H_{\text{vaporization}}$ (such as third-row metals), and therefore larger metal−metal bond energy leading (presumably) to smaller nuclei, is worth noting in this context (see Figures 8, 9 and 10 in ref 39). Overall, an important goal for future research is to study rationally, with the aim of obtaining a deeper understanding, the above and other factors which do (or do not) influence the kinetics of nanocluster formation, and hence, which also do (or do not) influence nanocluster final size.

In the case of literature systems (i.e., again ones not limited by micellar or other, templating environments),[7] there is already some experimental indication that nanocluster size is relatively insensitive to $[A]_0$ in the case of[45] Rh^0_n. Restated, the suggestion noted earlier that examining extremes of $[A]_0$ concentration, especially lower concentrations, in search of better size control when the two-step mechanism operates has some experimental

(42) Lin, Y.; Finke, R. G. *Inorg. Chem.* **1994**, *33*, 4891.
(43) Ott, L. S.; Hornstein, B. J.; Finke, R. G. *Langmuir* **2006**, *22*, 9357. see p. 9363−9364.
(44) Aiken, J. D., III; Finke, R. G. *J. Am. Chem. Soc.* **1998**, *120*, 9545.
(45) Tilley, T. D.; McMurdo, M.; Alivisatos, A. P.; unpublished results and experiments in progress (cited with permission). For related shape-control studies see: McMurdo, Meredith, J.; Alivisatos, A., Paul; Tilley, T., Don, Abstracts of Papers, 235th ACS National Meeting, New Orleans, LA, United States, April 6−10, 2008 (2008), INOR-1019 American Chemical Society, Washington, D. C.

support and, therefore, merits further examination. An important study in this regard is that of Tilley and co-workers showing that controlling precursor addition rate does allow some size (and shape) control in the case of Rh nanoparticles.[46] Another case worth noting is the insensitivity of Au^0_n prepared by Turkevich's $AuCl_3$/citrate^{3-} methods until values of $AuCl_3$/citrate^{3-} $\leq$ 2 or so are reached.[11] As noted briefly in the Introduction, this classic, aqueous system is actually quite complicated with it recently having been shown[14] that as the Na_3[citrate^{3-}]/$HAuCl_4$ ratio is changed, the pH is varying significantly and that, in turn, is changing the pH-dependent speciation of the $HAuCl_4$ nanocluster precursor, $[AuCl_{4-x}(OH)_x]^-$ ($x = 0$ at pH 3.3 to $x = 3$ at pH 8.1). With only pH control at a constant Na_3[citrate^{3-}]/$HAuCl_4$ ratio, nanoclusters from 20−40 nm were prepared in that 2007 study.[14] In another interesting study, Osterloh and Hiramatsu have reported a large-scale synthesis of 6−21 nm Au_n and 8−32 nm Ag_m nanoparticles with polydipersity as low as 6.9%.[47] Variation of the precursor and stabilizing amine concentrations were key to the size selectivity.[47]

In the case of Pd nanoclusters, Reetz and co-workers have demonstrated size control from 2.5 to 6.8 nm beginning with $Pd(NO_3)_2$ plus $R'_4N^+(RCO_2^-)$ functioning both as a reducing agent (and as a function of the oxidation peak potential of the RCO_2^-) and as a stabilizer.[48] The authors state that nucleation is faster than growth for the more reducing RCO_2^-, although dissection of the nucleation from the growth rate constants is not yet available to verify this probably correct claim for this interesting system. Reetz's laboratories have also demonstrated some size control via their electrochemical synthesis method of Pd, Ni, and Pt/Pd nanoclusters.[49] Finally, a recent book focusing on the issue of size control is available to the interested reader regarding what other factors are known to influence metal nanocluster size.[5]

9. The Sizes of Clusters Formed via the Four-Step, Double Autocatalytic Mechanism for Nanocluster Formation Which Includes Two Types of Nanocluster Agglomeration. Recently, we discovered a more general four-step mechanism for the nucleation, growth, and then agglomeration of transition-metal nanoclusters.[23,24] Because of the interest in the sizes of these agglomerated clusters, we attempted to extend the present treatment of nanocluster size vs time to systems which follow the four-step mechanism. Our initial treatment, and the problems inherent therein, are provided in the Supporting Information for the interested reader.

4. Conclusions

The main results and conclusions of this work are:

(1) The first kinetically supported, mechanism-based equation for transition-metal nanocluster formation size as function of time, D_t, was provided based on the two-step F−W mechanism (i.e., and for cases where the two-step mechanism has been shown to fit the nanocluster formation vs time kinetic data). The resultant eq 14 expresses the average[50] D_t as function of the average k_1, k_2, D_f, and the specific $[A]_0$. The involvement of the catalytically effective nucleus number, N^*, in the nanocluster size vs time equation is also noted via eq 20, and leads to the main drawback at present: the lack of an *ab initio* way to obtain N^* and its separate dependence on the k_1, k_2 and $[A]_0$ values. Hence, theoretical, direct detection and other efforts at obtaining N^* need to be a focus of future research efforts.

(2) Experimental size vs time data were obtained for a prototype Ir^0 nanocluster system, and that data was fit using eq 14, providing initial verification of eq 14. A noteworthy caveat here is that the precise relationship, if any, between N^* (as defined and used herein) and the classical critical nucleus number of nucleation theory[15–17] remains to be established.

(3) From eq 14, a way to convert from nanocluster size vs time to concentration vs time was derived, allowing one to obtain nucleation and growth rate constants from size vs time data.

(4) Equation 20 was used to estimate nucleus numbers for nine previously studied nanocluster systems, the results indicating that N^* decreases with increasing $k_2[A]_0/k_1$ ratios.

(5) Equation 14 and its derivatives, in turn, allow one to explore in a way more quantitative than heretofore possible the factors that change k_1 and k_2 with the goal of addressing rationally, and in a mechanism-supported way, the factors which affect these two key, nucleation and growth rate constants and the nanocluster size vs formation time that they help predict.

(6) Key other factors known at present to influence the size of transition-metal nanoclusters were cited (i.e., and in systems not constrained by micellar or other templates), including a recent book focused on the issue of size control.[5] These and other variables can now be studied systematically to show which rate constants (k_1 and/or k_2) are predominately affected, and hence how better size control can be achieved.

A number of studies remains to be performed. Further experimental verification of eq 14 and its derivatives remains to be accomplished, including for other transition-metal systems—although we expect the treatment herein to be more broadly applicable, including to other parts of Nature where the two-step, F−W mechanism has been shown to apply such as protein aggregation kinetics.[51] Studying the extremes of high and low $[A]_0$ is also suggested as a potentially useful avenue of achieving better size control. In addition, we know that there is probably in general a higher order, $k'_1[A]^n$, nucleation pathway than the first-order, $k_1[A]^1$, A→B mechanism (that higher order being kinetically hidden by the constant [A] in the induction period);[19] implications of this mechanistic change for the nanocluster size vs time profile are under study and will be reported in due course. Also needed are studies aimed at a kinetic determination of the (kinetically effective) nucleus number and its size as well as the *ab initio* prediction of the number of nuclei formed and, hence, the prediction of final nanocluster size.

It is our hope that the nanocluster community will help us test, and refine where necessary, this initial mechanism-based treatment and the equations presented herein. It is also our hope that the community can build off the results herein to attain better nanocluster size control in their own nanocluster syntheses and systems.

(46) Humphrey, S. M.; Grass, M. E.; Habas, S. E.; Niesz, K.; Somorjai, G. A.; Tilley, T. D. *Nano Letters* **2007**, *7* (3), 785–790.
(47) Hiramatsu, H.; Osterloh, F. E. *Chem. Mater.* **2004**, *16*, 2509–2511.
(48) Reetz, M. T.; Maase, M. *Adv. Mater.* **1999**, *11*, 773–777.
(49) Reetz, M. T.; Winter, M.; Breinbauer, R.; Thurn-Albrecht, T.; Vogel, W. *Chem. Eur. J.* **2001**, *7*, 1084–1094.
(50) (a) In this regard, the statement in the literature[50b] that the F-W mechanism "is unable to provide any information about the size *distribution* (italics added) of nanoclusters" is correct at present, since average k_1 and k_2 values are obtained from the two-step kinetic model. (b) D'Souza, L.; Suchopar, A.; Richards, R. M. *J. Colloid Interface Sci.* **2004**, *279*, 458.
(51) Morris, A. M.; Watzky, M. A.; Agar, J. N.; Finke, R. G. *Biochem.* **2008**, *47*, 2413–2427.

Acknowledgment. Discussions and collaboration with Professor T. Don Tilley at the University of California at Berkeley and Meredith McMurdo in his research group proved crucial in achieving the final form of this report, and are a pleasure to acknowledge. We also thank Mr. Joseph Mondloch and Ms. Aimee Morris for their assistance checking the equations herein and for offering critical comments on earlier versions which significantly improved the final form of the manuscript. Morgan Alley is thanked for his insightful comments that led to the term "catalytically effective nuclei" in place of other terms that were considered. This work was supported by the Chemical Sciences, Geosciences and Biosciences Division, Office of Basic Energy Sciences, Office of Science, U.S. Department of Energy, Grant Number DE-FFD02-03ER15453.

Supporting Information Available: Simplifications and assumptions underlying the Finke−Watzky two-step mechanism for transition-metal nanocluster nucleation and growth; mathematical treatment of the error propagation in eqs 15 and 20; initial treatment of nanocluster size vs time when the four-step mechanism is followed; and representative TEM images for the nanocluster size vs time experiments. This material is available free of charge via the Internet at http://pubs.acs.org.

JA8017412